In vivo biocompatibility and degradability of a Zn–Mg–Fe alloy osteosynthesis system

Xiaoxi Shao [a,1], Xiang Wang [a,e,1], Fangfang Xu [a,1], Taiqiang Dai [a], Jack G. Zhou [b,c], Jiang Liu [b], Kun Song [b], Lei Tian [a,**], Bin Liu [d,***], Yanpu Liu [a,*]

[a] *State Key Laboratory of Military Stomatology and National Clinical Research Center for Oral Diseases and Shaanxi Clinical Research Center for Oral Diseases, Department of Oral and Maxillofacial Surgery, School of Stomatology, The Fourth Military Medical University, 145 West Changle Road, Xi'an, 710032, PR China*
[b] *Hunan Huayao Bio Medical Technology Co., Ltd, Hunan, 410600, PR China*
[c] *Department of Mechanical Engineering and Mechanics, Drexel University, Philadelphia, PA, 19104, USA*
[d] *State Key Laboratory of Military Stomatology and National Clinical Research Center for Oral Diseases and Shaanxi Clinical Research Center for Oral Diseases, School of Stomatology, The Fourth Military Medical University, 145 West Changle Road, Xi'an, 710032, PR China*
[e] *The First Naval Hospital of Southern Theater Command, PLA, Zhanjiang, 524009, PR China*

ARTICLE INFO

ABSTRACT

Zinc is generally considered to be one of the most promising materials to be used in biodegradable implants, and many zinc alloys have been optimized to improve implant biocompatibility, degradation, and mechanical properties. However, long-term degradation leads to the prolonged presence of degradation products, which risks foreign body reactions. Herein, we investigated the *in vivo* biocompatibility and degradation of a biodegradable Zn–Mg–Fe alloy osteosynthesis system in the frontal bone, mandible, and femur in beagles for 1 year. Results of the routine blood, biochemical, trace element, and histological analyses of multiple organs, peripheral blood CD4/CD8a levels, and serum interleukin 2 and 4 levels showed good biocompatibility of the Zn–Mg–Fe alloy. Zinc content analysis revealed zinc accumulation in adjacent bone tissue, but not in the liver, kidney, and spleen, which was related to the degradation of the Zn–Mg–Fe alloy. The alloy demonstrated a uniform slowing degradation rate *in vivo*. No degradation differences in the frontal bone, mandible, and femur were observed. The degradation products included zinc oxide [ZnO], zinc hydroxide [$Zn(OH)_2$], hydrozincite [$Zn_5(OH)_6(CO_3)_2$], and hopeite [$Zn_3(PO_4)_2 \cdot 4H_2O$]. The good biocompatibility and degradation properties of the Zn–Mg–Fe alloy render it a very attractive osteosynthesis system for clinical applications.

1. Introduction

Zinc alloy is a new type of biodegradable material showing good biocompatibility, degradation properties, and mechanical strength [1–4]. Zinc is an essential trace element, required for the maintenance of physiological functions of the human body, and has osteogenic and antibacterial properties [5–7]. The corrosion potential of zinc is −0.76 V, which is between that of iron (−0.44 V) and magnesium (−2.37 V), and indicates a moderate degradation rate [8]. Pure zinc has poor mechanical properties; however, its ductility, strength, and degradation

properties can be improved by alloying. Zinc alloys possess improved mechanical strength (up to 200 Mpa), which is sufficient for bone implants [9]. The above traits of zinc alloy make it a promising candidate for medical biodegradable material.

Previously, we studied a Zn–Mg–Fe alloy used as an osteosynthesis system in a canine mandibular fracture model [10]. Our preliminary findings indicated that the Zn–Mg–Fe alloy provides good mechanical strength to support bilateral mandible fracture healing during a 24-week observation period. The main purpose of the previous study was to explore the efficacy of Zn–Mg–Fe alloy osteosynthesis system in

---

mandibular fracture, and the biocompatibility and degradation of zinc alloy *in vivo* was only preliminarily explored.

Because of the biodegradability of the zinc alloy, the continuously released metal ions may be toxic to the body in the long term, e.g., affecting the blood, and digestive, nervous, and immune systems [11]. Furthermore, prolonged zinc exposure may lead to copper deficiency, characterized by hypokalemia, anemia, leukopenia, and neutropenia [12]. Further, competition between zinc and iron can lead to decreased serum ferritin and hematocrit levels [13]. In addition, excessive zinc adversely affects serum cholesterol balance, which is usually characterized by an increase in low-density lipoprotein levels and a decrease in high-density lipoprotein levels [14]. Chronic zinc intake may lead to impaired pancreatic function, resulting in increased release of amylase, lipase, and alkaline phosphatase in the blood [15]. Microscopic hematuria without renal failure and mild proteinuria are associated with high-dose zinc intake. Excessive zinc intake can also be characterized by increased liver enzyme activity [16]. Changes in zinc levels in the brain can lead to a series of neurological disorders, such as impaired brain development, neurodegenerative disorders, including Alzheimer's disease and depression, and neuronal damage associated with traumatic brain injury, stroke, and seizure [17,18]. Furthermore, serum zinc concentrations in benign prostatic hyperplasia patients are significantly higher than those in normal controls [19]. Finally, excessive zinc intake can inhibit the activity and phagocytosis of immune cells and the immune function of the body [20]. Therefore, the biocompatibility of zinc alloy implants should be investigated in detail *in vivo*.

The degradation process of degradable metals depends on the internal environment, as electrolytes accelerate the degradation rate, and the degradation of degradable materials varies at different implantation sites [21,22]. For instance, the local blood flow, water content of different tissues, and different mechanical loading may result in different degradation patterns [23]. Mirua et al. [21] reported that the rate of Mg-1.0Al corrosion in their study was the fastest in the subperiosteum head and the slowest in the muscle of the rat femur. The rate was intermediate in the subcutaneous tissue in the back. Whether it is necessary to design different degradable osteosynthesis systems with different composition or processing for different anatomical sites remains to be determined. The frontal bone, mandible, and femur can be tested as implantation sites to evaluate the degradation of implant material *in vivo*, as these sites are potential osteosynthesis system implantation sites in the clinic. In addition, the anatomical structures of frontal bone, mandible, and femur are quite different and representative (Table 1) [24].

The current study was devised to comprehensively analyze the biocompatibility and degradation properties of the Zn–Mg–Fe alloy after implantation, *in vivo*, for 1 year. We used beagle as the animal model, and simultaneously implanted four sets of standard-sized Zn–Mg–Fe alloy osteosynthesis systems in the frontal bone, bilateral mandible, and femur. We anticipated that the degradation rate would be different at these implantation sites. Further, the current study was devised as a preclinical study. The plates and screws used were standard-sized and can be directly clinically applied in human. Using a series of biochemical and biophysical approaches, we show that the Zn–Mg–Fe alloy has very good biocompatibility and degradation properties *in vivo*, making it an attractive osteosynthesis system for clinical applications.

Table 1
Anatomy of different implantation sites.

Implantation site	Anatomy (from the inside to the outside)
Frontal bone	Frontal bone, periosteum, frontalis, thin subcutaneous tissue, skin
Mandible	Mandible, periosteum, thin layers of muscle, thin submucous tissue, mucous membrane
Femur	Femur, periosteum, thick layers of muscle, thick subcutaneous tissue, skin

2. Materials and methods

2.1. Experimental animals

All animal procedures and experiments were reviewed and approved by the Institutional Animal Care and Use Committee at The Fourth Military Medical University [Xi'an, China; ethical review number 2017 (kq-008)]. All procedures were performed in full compliance with the institutional and national animal protection laws, and were approved by the local animal welfare committee. Twenty-four mature and healthy beagles (12 male and 12 female; body weight of 11–13 kg) were randomly assigned to four groups for implantation and observation 3, 6, 9, and 12 months post surgery. Each group contained three male and three female dogs.

2.2. Preparation of materials

The prototype Zn–Mg–Fe alloy fixation plates used were standard-size, four-hole plates, 1-mm thick and 28.6-mm long. The cortical bone screws were 7-mm long and had a 2-mm shaft diameter. All plates and screws were from Hunan Huayao Bio Medical Technology Co., Ltd, China. The Zn–Mg–Fe alloy composition was as follows: 98 wt%$\leq$Zn $\leq$ 99.5 wt%, 0.01 wt%$\leq$Mg $\leq$ 0.5 wt%, and 0.01 wt% $\leq$Fe $\leq$ 0.5 wt%. The Zn–Mg–Fe alloy was prepared from high-purity Zn (99.995 wt%), Mg (99.99 wt%), and Fe (99.9 wt%). The material was melted and mixed in a medium-frequency induction furnace to cast as ingots. An electromagnetic stirrer was used to homogenize the melt, and 99.999% argon was used as a protection gas to prevent oxidation and achieve the desirable alloy composition. The ingots were extruded at 200 °C and 15–20 mm/s, with an extrusion ratio of 14:1–16:1, and drawn to 5–10-mm diameter rods. The screws for the *in vivo* animal study were made from as-extruded rods. The ingots were forged at 200 °C and cold-rolled into 0.5–1.5 mm-thick plates. The tensile strength of the plates (n = 15) and screws (n = 15) was 265.1 $\pm$ 2.84 MPa and 316.1 $\pm$ 3.82 MPa, respectively. All screws and plates were sterilized under 25 kGy ^{60}Co radiation.

2.3. Surgical procedures

All beagles were anesthetized using an intramuscular injection of xylazine hydrochloride (0.1 mL/kg) and 3% pentobarbital (0.3 mL/kg). Lidocaine with epinephrine was administered at the surgical sites for local anesthesia. The center of the frontal bone, the left and right side of the mandible, and the middle part of the right femur were chosen as the implant sites in each beagle. A Zn–Mg–Fe alloy plate and screw were implanted at each site. The screws that fixed the plate to the frontal bone were 2 mm shorter than the other screws, to accommodate the relatively small frontal bone thickness. Water and food were supplied *ad libitum*. For the first 3 d following the surgery, 8×10^5 units of penicillin was administered intramuscularly to each beagle, twice daily. The animals were examined every day, and the wound healing and general status were recorded.

2.4. Hematological analysis

Hematological analyses were conducted before the surgery, and 3, 6, 9, and 12 months post surgery. For routine blood, biochemical, and trace element analyses, the blood was collected in tubes containing EDTA as an anti-coagulant, tubes without any additives, and tubes containing heparin as an anti-coagulant, respectively. In addition, the collected blood without any additives was kept in a tube for 30 min and then centrifuged (4000 rpm for 8 min) to separate the serum. Routine blood tests, such as the determinations of the counts of white blood cells (WBC), red blood cells (RBC), platelets (PLT), hemoglobin (Hb), and monocytes, were performed using the Sysmex SE-9000 automatic hemocyte analyzer (DKK-TOA, Japan). Blood biochemical tests, including

the measurements of the alanine amino transferase (ALT), aspartate transaminase (AST), alkaline phosphatase (ALP), albumin (ALB), total protein (TP), creatinine (CRE), blood urea nitrogen (BUN), total cholesterol (CHOL), triglyceride (TG), low-density lipoprotein (LDL), and high-density lipoprotein (HDL) levels were performed using a 7600P automatic biochemical analyzer (Hitachi, Japan). Blood trace element analyses, including those for determining zinc, magnesium, iron, calcium, and copper levels, were performed using the BH5300 whole-blood multi-element analyzer (bohui-tech, China).

2.5. Histological analysis

The following tissues were processed for histological analysis 12 months post surgery: tissues retrieved from the heart, liver, spleen, lung, kidney, testis, epididymis, prostate, uterus, ovary, oviduct, hypophysis, pancreas, adrenal, submandibular, thyroid, and parathyroid glands; the cerebrum; tissues adjacent to the frontal bone, mandible, and femur; and the fontal bone, mandible, and femur. The specimens were fixed in 4% neutral buffered formalin for 48 h. The frontal bone, mandible, and femur samples were fixed, dehydrated, and cleared in xylene. The bones were then infiltrated and embedded in methyl methacrylate, and 200-μm thick sections were obtained, which were subsequently ground to a thickness of 50 μm. All sections were stained in Van Gieson's picrofuchsin stain. Other soft tissues were dehydrated in graded ethanol, cleared in xylene, embedded in paraffin, and sectioned into 5-μm slices. All sections were stained using hematoxylin and eosin.

2.6. Zinc content analysis

One side of the mandible was randomly selected for zinc content analysis. The liver and kidney tissues were also harvested for zinc content analysis. Zinc concentration was determined using inductively-coupled plasma optical emission spectrometry (PerkinElmer Optima 8000, USA). Samples were digested using 6 mL of nitric acid and 2 mL of hydrochloric acid in Teflon® containers. They were then heated in a microwave (MARS6, CEM Corporation, USA), and diluted with 50 mL of highly purified water in polypropylene tubes. The zinc content of the samples was subsequently analyzed using inductively coupled plasma optical emission spectrometry.

2.7. Immunological analysis

2.7.1. Flow cytometry

The assessment of immune cell subsets in beagle peripheral blood was performed using flow cytometry. EDTA-whole blood mixture (90 μL) was mixed with 5 μL of APC rat anti-dog CD8a (eBioscience, Thermo Fisher, USA) and 5 μL of FITC rat anti-dog CD4 (eBioscience) monoclonal antibodies. The samples were incubated for 20 min at room temperature in the dark. Following the addition of the BD FACSTM lysing solution, cells were collected by centrifugation (1500 rpm, 5 min), washed and resuspended in phosphate-buffered saline, and analyzed using a FACScan flow cytometer (BDFACSCanto II, USA).

2.7.2. Enzyme-linked immunosorbent assay (ELISA)

ELISA was employed to measure the interleukin (IL) 2 and 4 levels in peripheral blood. Briefly, peripheral blood was obtained and allowed to clotted. The serum was obtained by centrifugation at 4000 rpm for 8 min at room temperature, and then frozen at −80 °C until use. The IL-2 and IL-4 levels were measured using an ELISA kit (Shanghai Sangon Biotech, Inc., Shanghai, China). All measurements were performed according to the manufacturer's instructions.

2.8. Micro-computed tomography (micro-CT)

The frontal bone, mandible, and femur were harvested after euthanasia, 3, 6, 9, and 12 months after the surgery. The samples were fixed in

4% paraformaldehyde for 48 h and micro-CT analysis was performed. One randomly selected side of the mandible, frontal bone, and femur of each beagle was scanned using a microtomography imaging system (YXLON Y. Cheetah, Germany). The micro-CT system had a maximum voltage of 120 kV and current of 41.0 μA. Three-dimensional imaging and volume loss of the implants were evaluated using the three-dimensional image processing software VG Studio Max 3.0 (Volume Graphics, Heidelberg, Germany).

The *in vivo* corrosion rate (CR) of the Zn–Mg–Fe alloy was calculated using the following equation [25]:

$$CR = \frac{\triangle V}{A.t}$$

where CR is the corrosion rate (mm y^{-1}); $\triangle V$ is the volume loss (the Zn–Mg–Fe alloy volume before implantation minus the remaining volume [mm^3]); A is the surface area (mm^2); and t is the implantation time (y).

2.9. Scanning electron microscopy (SEM)

Following micro-CT scanning, each sample was cut into two blocks, one for SEM surface scanning analysis and the other for embedding in methyl methacrylate. Then, the blocks were cut into 1-mm–thick sections using a diamond saw (Leica SP1600, Leica Instruments, Nussloch, Germany). All samples were coated with a thin layer of gold (SHINKKU VD MSP 1S, Japan) to improve conductivity prior to imaging and imaged using an SEM (S-4800, Hitachi, Japan). Representative corrosion regions in all samples were further analyzed using an energy-dispersive X-ray spectroscope (EDS, Oxford, UK). Surface morphology of the Zn–Mg–Fe alloy 12 months post implantation and after removing degradation products was analyzed by SEM. Briefly, samples were treated with chromic acid (200 g CrO_3 and 10 g $AgNO_3$ in 1000 mL of distilled water) by immersing for 5 min with ultrasonic vibration to remove degradation products. Afterwards, the samples were cleaned in 100% ethanol with ultrasonic vibration for 5 min, air-dried, and analyzed by SEM.

2.10. Degradation product analysis

Degradation products on the plates and screws were gently scraped off and rinsed with double distilled water. After drying at 40 °C for 12 h, they analyzed as described in sections 2.10.1 to 2.10.3.

2.10.1. X-ray photoelectron spectroscopy (XPS)

The degradation products were analyzed using XPS (ESCALAB, Thermo Fisher, USA) with and an Al–Kα source at a step size of 1 eV. High-resolution narrow scans were analyzed at a step size of 0.1 eV.

2.10.2. Fourier-transform infrared (FTIR) spectroscopy

FTIR spectroscopy (VERTEX 70, Bruker, Germany) was employed to identify the functional groups of degradation products. A series of 64 scans were performed at 4 cm^{-1} resolution in the range of 400–4000 cm^{-1}.

2.10.3. X-ray diffraction (XRD)

The chemical composition of implant degradation products was characterized using XRD (SmartLab, Rigaku, Japan) and CuKα with an angle at a scanning speed of 5°/min in the 2θ range of 10–90°.

2.11. Statistical analysis

The results are presented as the means ± standard deviations (SDs). The data were analyzed using SPSS 19.0 (SPSS Inc., Chicago, USA). Statistical significance was assessed using one-way analysis of variance (ANOVA), followed by the Tukey's test. A *p*-value less than 0.05 was

considered statistically significant.

3. Results

3.1. Biocompatibility of the Zn–Mg–Fe alloy

3.1.1. General observations

In general, the surgical procedure and the Zn–Mg–Fe alloy osteosynthesis material were well tolerated by the beagles. There were no signs of local inflammation, healing disturbance, allergic reactions, or other complications. With time, the surface of the Zn–Mg–Fe alloy osteosynthesis material became increasingly corroded, with an increasing number of white granular degradation products (Fig. S1). New bone covering the Zn–Mg–Fe alloy was also observed.

3.1.2. Hematological analysis

The possibly high levels of zinc ions released from the Zn–Mg–Fe alloy into the circulation might pose a biosafety concern. Therefore, routine blood, biochemical, and trace element analyses were performed before and after the surgery. Regarding the routine blood tests, the levels of WBC, RBC, PLT, Hb, and monocytes were all within the normal range in the Zn–Mg–Fe alloy-implanted animals, with no statistically significant differences before and after the surgery ($p > 0.05$) (Fig. 1). With regard to the blood biochemistry testing, no abnormalities in the levels of ALT, AST, ALP, ALB, TP, CRE, BU, CHOL, TG, LDL, and HDL were noted during the observation period, and all values fluctuated within the normal range. No statistically significant differences were apparent between the time points ($p > 0.05$) (Fig. 1). Further, the blood zinc,

magnesium, iron, calcium, and copper concentrations were maintained at normal level and did not show significant increases during the observation time compared to the levels prior to the surgery (Fig. 2). This indicated that the degradation of the Zn–Mg–Fe alloy did not lead to significantly elevated concentrations of zinc in the blood, and did not perturb the metabolism of magnesium, iron, copper, and calcium. No statistically significant differences ($p > 0.05$) were noted in the post-surgical levels of these elements compared to those before the surgery. Collectively, the analyses indicated that the use of the Zn–Mg–Fe alloy was not associated with an increased blood zinc concentration, and did not cause abnormal alterations in routine blood and biochemical indicators, demonstrating the good *in vivo* biosafety performance of the Zn–Mg–Fe alloy material.

3.1.3. Histological analysis

To identify histological changes, we harvested various tissues from the animals 12 months after implantation and evaluated tissue histology. Tissue section morphologies are shown in Fig. 3. No morphological changes were apparent in the harvested tissues, no inflammatory cell infiltration, and no destruction of the tissue structure. No observable pathologies were identified, which indicated that the implantation of the Zn–Mg–Fe alloy did not result in systemic toxicity.

3.1.4. Zinc content analysis

With the degradation of the Zn–Mg–Fe alloy, zinc might accumulate in organs, such as the liver, kidney, and spleen. Accordingly, we measured the zinc content in these tissues, as well as in the bone tissue proximal to the implantation sites, at various time points after
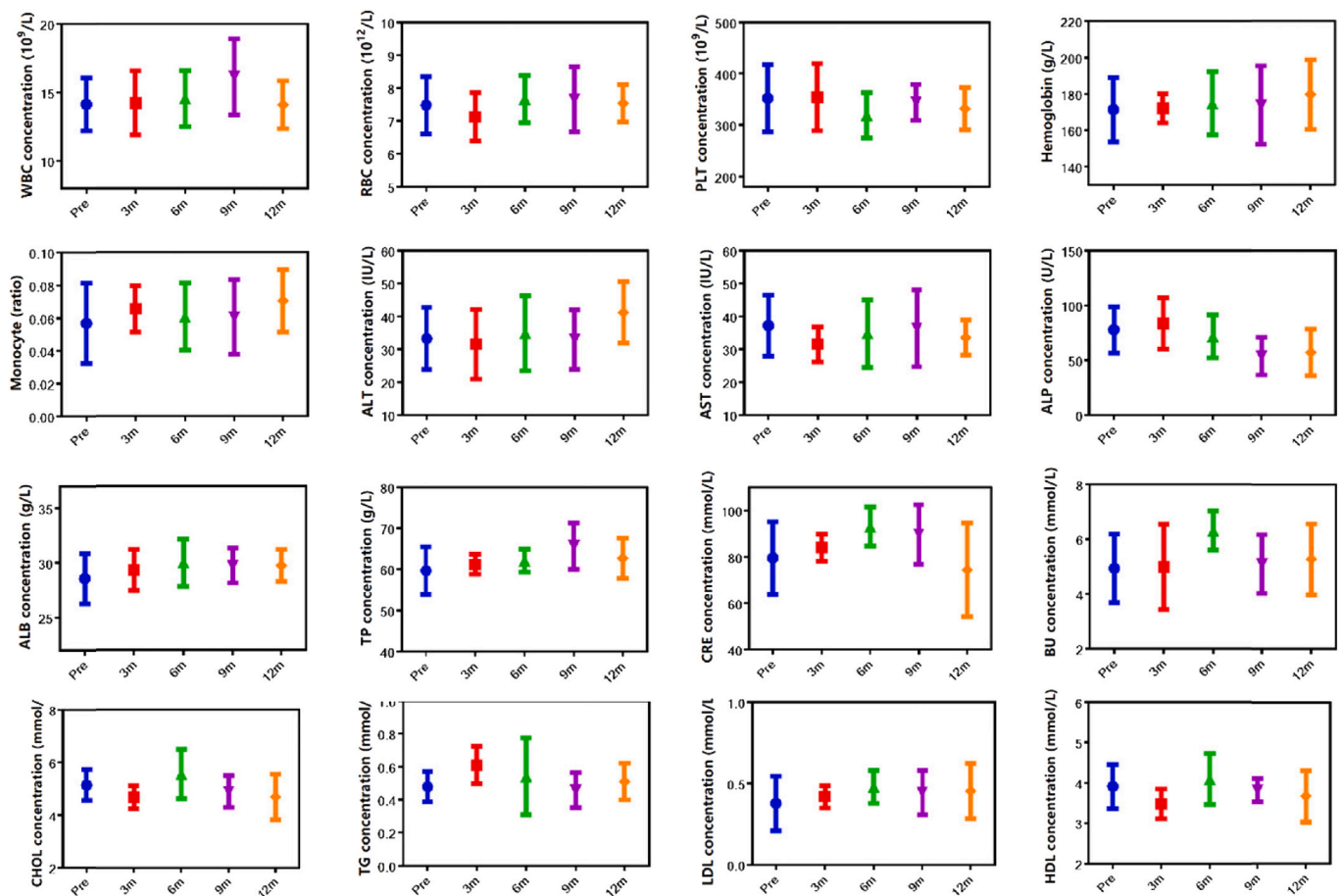

Fig. 1. Routine blood and biochemistry tests data before and after implantation of the Zn–Mg–Fe alloy. For each data point, six samples were analyzed in duplicate, and the mean values ± SDs are presented. The abbreviations are as explained in section 2.4. No statistically significant differences were observed between the time points ($p > 0.05$).
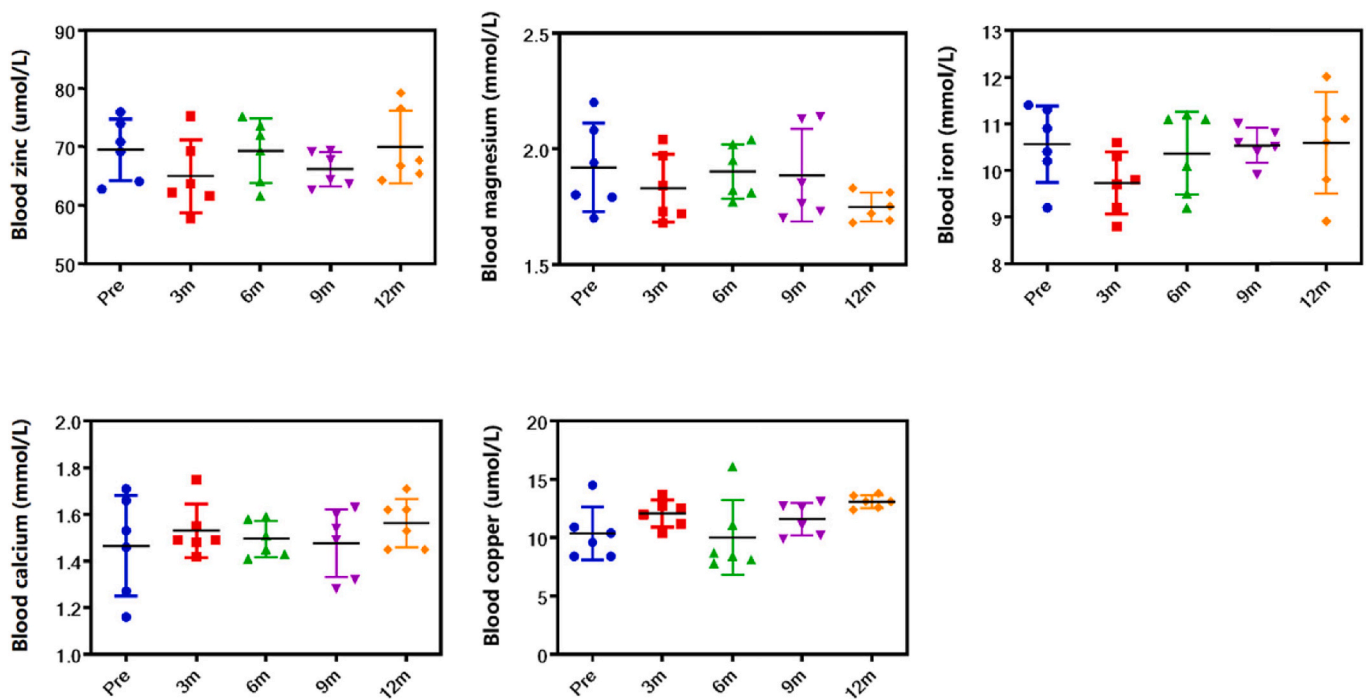
Fig. 2. Blood zinc, magnesium, iron, calcium, and copper concentrations before and after implantation of the Zn–Mg–Fe alloy. For each data point, six samples were analyzed in duplicate, and the mean values ± SDs are presented. No statistically significant differences were observed between the time points ($p > 0.05$).

implantation (Fig. 4). No significant differences were detected in the zinc content of the liver, kidney, and spleen ($p > 0.05$). This indicated that the *in vivo* zinc balance was not perturbed by the degradation of the Zn–Mg–Fe alloy and that zinc released from the implant was metabolized, instead of continuously accumulating in the organs. On the other hand, the zinc contents in the adjacent bone tissue increased after implantation, with the highest levels being observed 3 months after the surgery; the levels showed a downward trend after the 3-month time point.

3.1.5. Immunological analysis

3.1.5.1. Flow cytometry analysis.
We analyzed the peripheral blood CD4/CD8a ratios to identify immune response of Zn–Mg–Fe alloy implanted *in vivo*. No significant differences were apparent between the time points analyzed ($p > 0.05$) (Fig. 5A), indicating limited immune responses of Zn–Mg–Fe alloy.

3.1.5.2. ELISA.
We next determined serum levels of the immune response indicators IL-2 and IL-4 before and after implantation (Fig. 5B and C). No statistically significant differences in the IL-2 and IL-4 levels were apparent between the different time points analyzed ($p > 0.05$), indicating that the release of zinc into the circulation did not induce any immune responses.

3.2. Degradation of the Zn–Mg–Fe alloy in vivo

3.2.1. Micro-CT analysis
Micro-CT scanning revealed that the surface of the Zn–Mg–Fe alloy plates and screws became rough and corroded with time, but that the shape outline of the implants remained nearly intact throughout the experimental period (Fig. 6A, Fig. S2). The volume of the Zn–Mg–Fe alloy implants was analyzed using the VG-studio 3.0 software (Fig. 6B). No statistically significant differences between the frontal bone, mandible, and femur implant volume loss at the same time points were noted ($p > 0.05$). Further, the implants in the frontal bone, mandible, and femur showed volume loss of 19.20 ± 1.25%, 18.43 ± 0.53%, and

19.06 ± 1.08%, respectively, 12 months after the implantation. The CR values of the frontal bone, mandible, and femur implants gradually decreased over time (Fig. 6C, Table 2). The CR values of the implants in the first 3 months post surgery were higher than those in the last 9 months analyzed. No statistically significant differences in the volume loss or CR values between the Zn–Mg–Fe alloy pieces implanted in the frontal bone, mandible, and femur at the same time points were noted ($p > 0.05$) (Fig. 6B, C, Table 2).

3.2.2. SEM analysis
Surface morphology of the Zn–Mg–Fe alloy implanted in the frontal bone, mandible, and femur 3, 6, 9, and 12 months after implantation is shown in Fig. 7. In the images, the surface is covered with a layer of degradation products. The degradation products displayed a variety of morphologies, with some surface cell adhesion and tissue infiltration visible. EDS analysis revealed that the degradation products contained Zn, O, C, P, Ca, Cl, N, Na, and K (Fig. S3). As shown, the composition of the degradation products varied with the different degradation morphologies, suggesting the existence of a complex degradation microenvironment *in vivo*. The corroded surface of Zn–Mg–Fe alloy is shown in Fig. S4. Irregular and small pits were observed after removal of the degradation products.

Representative SEM morphologies of the cross-sections of the Zn–Mg–Fe alloy in the frontal bone, mandible, and femur 12 months post surgery are shown in Fig. 8. A corresponding element mapping revealed a favorable uniform macroscopic degradation, with small, shallow cracks visible after 12 months post surgery. This contrasted with a severe localized pitting and crevice corrosion reported for Mg alloys [26].

Corrosion products were visible and distributed around the implant (Fig. 8). The interface consisted of a residual Zn–Mg–Fe alloy, degradation products, and bone. The EDS mapping revealed that the bone was rich in Ca and P, and the degradation products were rich in Zn and O. In the femur section, Ca and P were observed in some parts of the degradation layer, which indicated that new bone appeared in the degradation product layer.
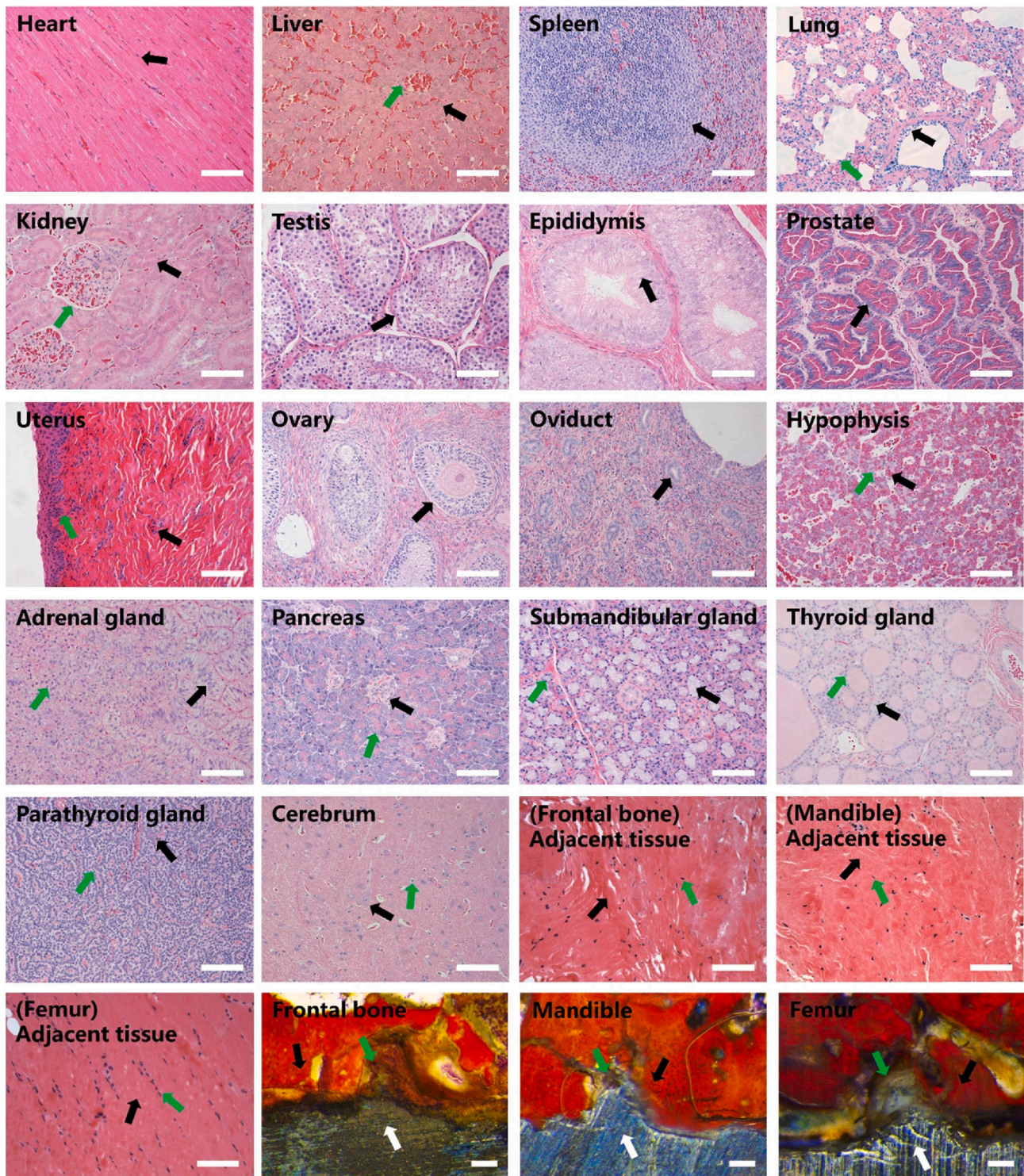
Fig. 3. Histological analysis of various tissues 12 months after surgery. The following are shown: tissues harvested from the heart (black arrow: cardiac myocytes), liver (black arrow: hepatocyte; green arrow: hepatic interlobular vein), spleen (black arrow: lymphatic nodule), lung (black arrow: terminal bronchiole; green arrow: pulmonary alveolus), kidney (black arrow: renal tubules; green arrow: glomerulus), testis (black arrow: seminiferous tubule), epididymis (black arrow: chief cell), prostate (black arrow: glandular epithelial cell), uterus (black arrow: uterine gland; green arrow: uterine epithelium), ovary (black arrow: ovarian follicle), oviduct (black arrow: secretory cell), hypophysis (black arrow: acidophil; green arrow: chromophobe cell), adrenal gland (black arrow: cells in the fascicular zone; green arrow: cells in the reticular zone), pancreas (black arrow: pancreatic islet; green arrow: pancreatic acinus), submandibular gland (black arrow: mucous acinus; green arrow: serous acinus), thyroid gland (black arrow: parafollicular cell; green arrow: follicular epithelial cell), parathyroid gland (black arrow: oxyphil cell; green arrow: chief cell), cerebrum (black arrow: pyramidal cell; green arrow: oligodendrocyte), frontal bone adjacent tissue (black arrow: collagenous fiber; green arrow: fibrocytes), mandible adjacent tissue (black arrow: collagenous fiber; green arrow: fibrocytes), femur adjacent tissue (black arrow: muscle fiber; green arrow: nucleus of muscle fiber), fontal bone (black arrow: bone; green arrow: degradation product; white arrow: Zn–Mg–Fe alloy), mandible (black arrow: bone; green arrow: degradation product; white arrow: Zn–Mg–Fe alloy), femur (black arrow: bone; green arrow: degradation product; white arrow: Zn–Mg–Fe alloy). Scale bar = 100 μm.
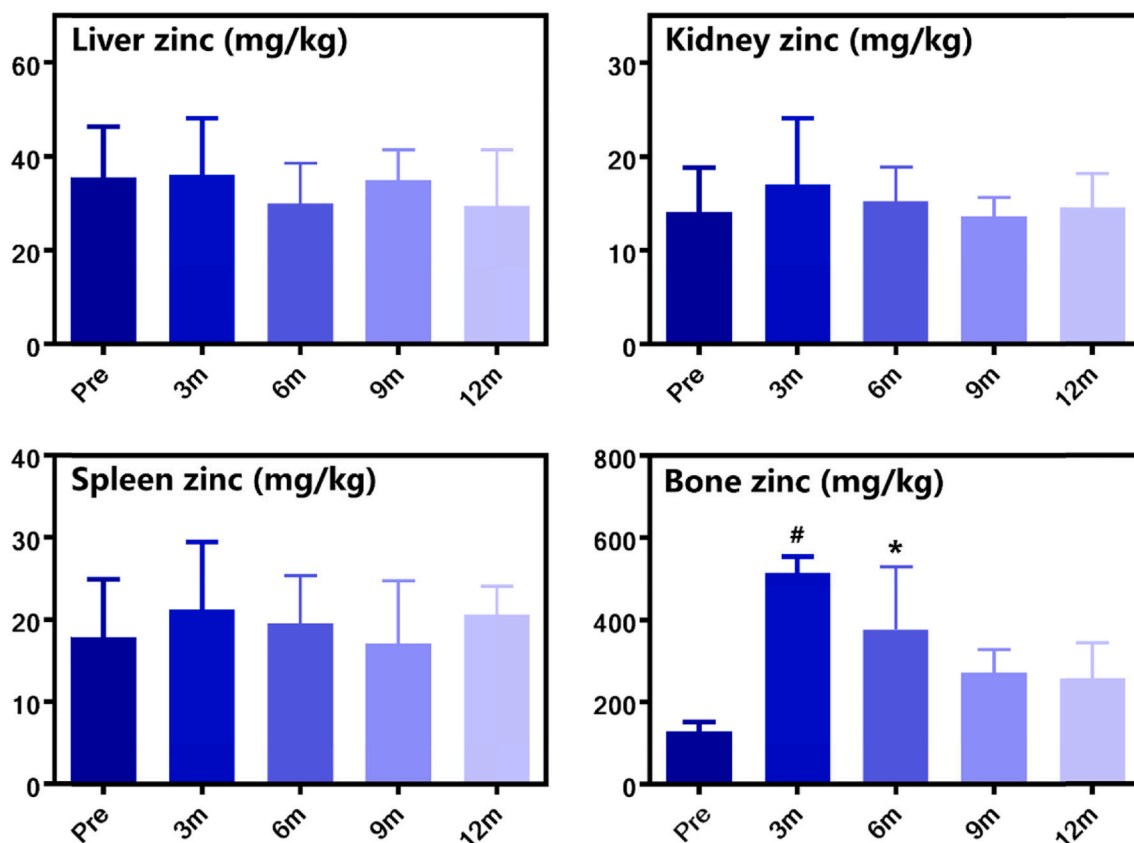
Fig. 4. Zinc content of the liver, kidney, spleen, and adjacent bone tissue. For each data point, six samples were analyzed in duplicate, and the mean values $\pm$ SDs are presented. No statistically significant differences were observed between the time points in the liver, kidney, and spleen samples ($p > 0.05$). Zinc content in the adjacent bone tissue was significantly elevated 3 and 6 months post surgery (*$p < 0.05$ vs. pre-surgery; #$p < 0.05$ vs. pre-surgery or 9 months or 12 months post surgery).

3.2.3. Degradation products

The results of XPS, FTIR, and XRD analyses of the Zn–Mg–Fe alloy 12 months after implantation are shown in Fig. 9. According to the XPS analysis, the corrosion products primarily comprised Zn, O, C, P, Ca, Na, and N (Fig. 9A). The presence of N may be attributable to the infiltration of biological tissues. High-resolution Zn $2p_{3/2}$ spectra are shown in Fig. S5. Peaks located at 1021 eV were assigned to Zn [27]; those at 1021.2 eV were related to $Zn_3(PO_4)_2 \cdot 4H_2O$ [28]; peaks at 1022.5 eV indicated the existence of $Zn(OH)_6(CO_3)_2$ [29]; and those at 1022.8 eV were attributed to $Zn(OH)_2$ [29].

FTIR spectra from the different implantation sites are shown in Fig. 9B. The absorption band in the 3100–3600 cm^{-1} region was attributed to the O–H stretching vibration [30]. The peaks at 1645 cm^{-1} were related to the H_2O bending vibration [31]. The 1400–1500 cm^{-1} range corresponded to the v_3 mode of CO_3^{2-} [31]. The narrow and high intensity peaks observed at 1000–1140 cm^{-1} corresponded to the v_3 mode of PO_4^{3-}, and peaks at 560–580 cm^{-1} were assigned to the v_4 vibrational mode of PO_4^{3-} [31]. The peak at approximately 580 cm^{-1} was most likely related to ZnO [32]. Furthermore, some absorption bands indicated the presence of organic substances [33]. The peak at 3300 cm^{-1} was related to N–H stretching. The peak at 2920 cm^{-1} indicated the H–C stretching [34]. The peak at approximately 1650 cm^{-1} was assigned to amide I vibration and the peak at 1535 cm^{-1} was related to amide II vibration. The peak close to 1395 cm^{-1} was associated with the symmetric stretching of COO. The peak at approximately 1235 cm^{-1} was assigned to amide III vibration. Finally, the broad band near 1100 cm^{-1} could be attributed to C–C or C–O stretching.

The XRD analysis revealed diffraction peaks corresponding to zinc oxide [ZnO, PDF file 03-065-0682], zinc hydroxide [$Zn(OH)_2$, PDF file 01-074-0094], hydrozincite [$Zn_5(OH)_6(CO_3)_2$, PDF file 01-072-1100], and hopeite [$Zn_3(PO_4)_2 \cdot 4H_2O$, PDF file 01-074-2275] (Fig. 9C).

4. Discussion

The aim of the current study was to investigate the biocompatibility and degradability of a biodegradable Zn–Mg–Fe alloy osteosynthesis system. We showed that the alloy is not toxic, has desirable biodegradability traits, and is a promising candidate material to be used in the clinic.

Good biocompatibility is an essential property of medical implants. Zinc is an essential trace element for human. The recommended daily intake of zinc is 107–231 μmol d^{-1}, the daily requirement of zinc is 15 mg d^{-1}, and the tolerable upper intake level is 40 mg d^{-1} [35]. As a degradable metal, its release during the long-term degradation of the zinc alloy may have harmful effects on the human body. However, we showed here that Zn–Mg–Fe alloy osteosynthesis system is safe for use in the body.

Specific indices determined in the course of routine blood and biochemistry analyses, which are sensitive to many pathological changes in the body, are commonly used as indicators of the physiological and pathological state. Blood trace element indices are an effective way for monitoring zinc levels in the circulation and degradation of the Zn–Mg–Fe alloy *in vivo*. In the current study, we observed that some indicators fluctuated within the normal range, or showed specific trends; however, no statistically significant differences were observed, indicating the absence of serious blood cell abnormalities, hepatic or renal dysfunction, and metabolic lipid or trace element disorders during the alloy implantation.

Excessive zinc intake may be toxic to the kidney, liver, and cardiovascular, nervous, and immune systems [36–38]. However, we did not
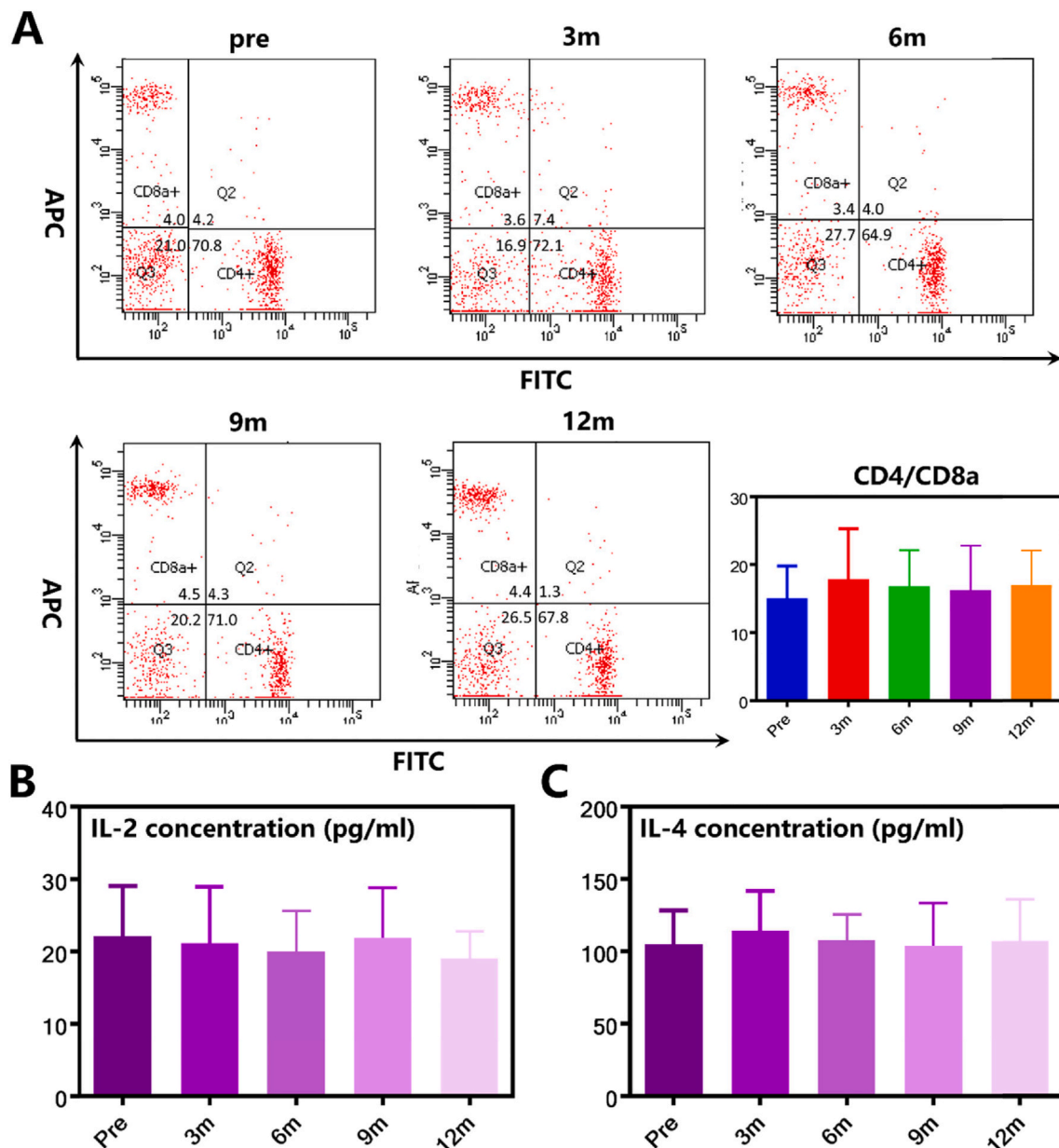
Fig. 5. Effect of the Zn–Mg–Fe alloy on the immune system. (A) Peripheral blood CD4/CD8a ratios at different time points after implantation. (B) Interleukin (IL) 2 and (C) IL-4 concentrations before and after implantation of the Zn–Mg–Fe alloy. For each data point, six samples were analyzed in duplicate, and the mean values ± SDs are presented. No statistically significant differences were observed between the time points ($p > 0.05$).

observe any pathologies in the inner organs of beagle during Zn–Mg–Fe alloy degradation, which is consistent with the blood test results, suggesting that the Zn–Mg–Fe alloy has good *in vivo* biocompatibility.

In the current study, the liver, kidney, spleen, and adjacent bone tissues were retrieved for zinc content analysis. Rössig et al. [39] systematically investigated the accumulation of rare earth elements in the liver, kidney, and spleen in sheep 24 weeks after implantation of a LAE442 magnesium-based intramedullary interlocked nailing system. The amounts of rare earth elements in these organs were significantly higher than those in the stainless austenitic steel 1.4441LA group; however, no histopathological changes were observed. In the current study, the biodegradation rate of the implanted alloys had no measurable effect on the zinc content of different organs.

Zinc released during degradation can be absorbed by the surrounding tissues [40] and excreted via the gastrointestinal route and the kidney [35]. Consequently, we also investigated changes in zinc concentration in the adjacent bone tissue. We showed that the zinc content

therein was the highest 3 months post surgery, and then exhibited a decreasing trend. This may have coincided with the degradation rate of the Zn–Mg–Fe alloy, suggesting that a high degradation rate increases the local concentration of elements; as the degradation rate decreases and stabilizes, these elements are slowly metabolized. In one study [41], degradation of the Mg alloy led to an increased Mg concentration in the cortical bone near an implant, but returned to normal levels after complete degradation of the implant. As we did not analyze the complete degradation of the Zn–Mg–Fe alloy in the current study, zinc metabolism in bone tissue after complete implant degradation should be investigated further.

Zinc is essential for many facets of the immune system, including the normal development, differentiation, and function of cells involved in the innate and acquired immune responses [42,43]. T lymphocytes are immune cells most susceptible to zinc deficiency. Disrupted zinc homeostasis negatively affects the immune system, resulting in a weakened formation, activation, and maturation of immune cells [44]. This can
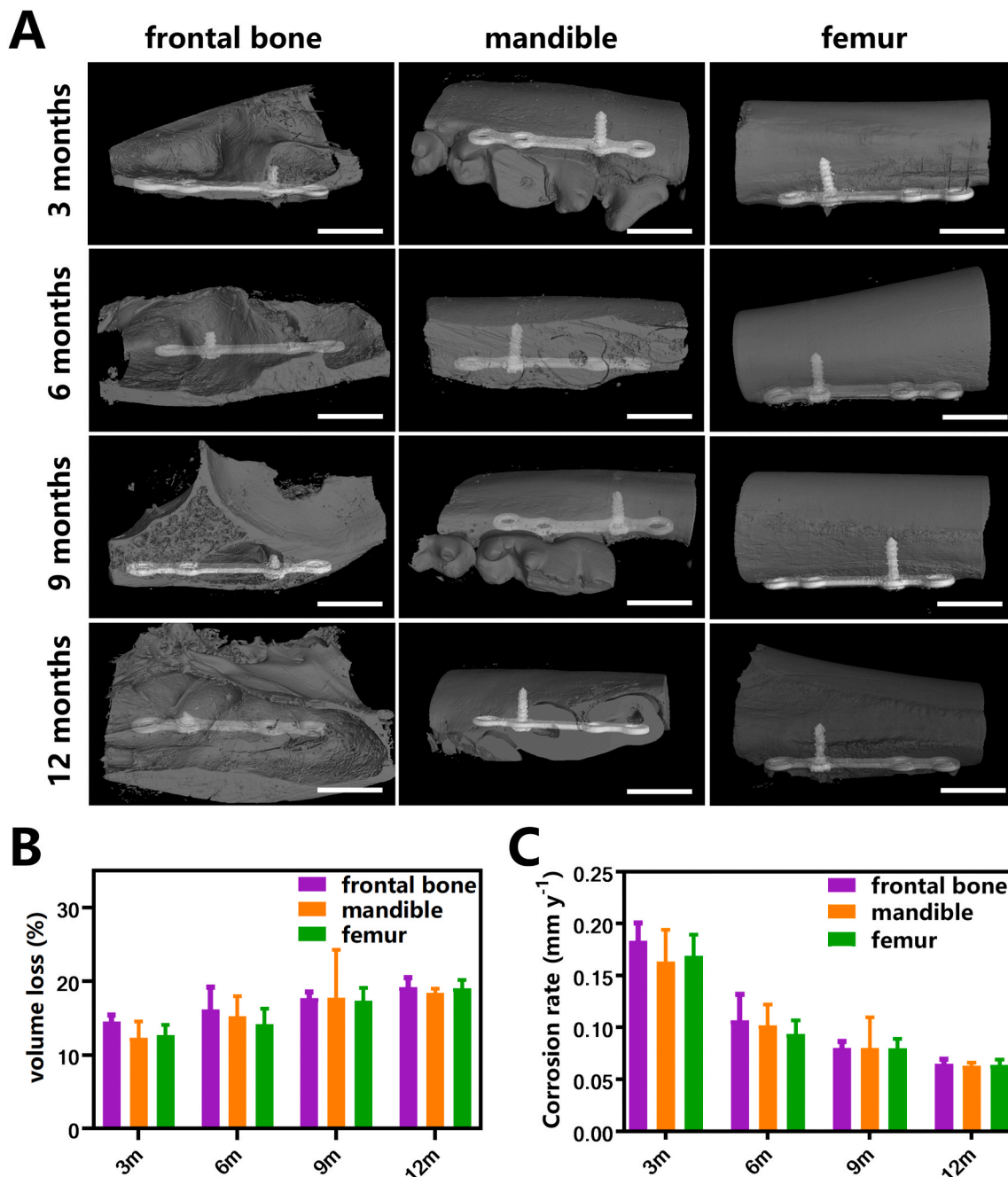
Fig. 6. Analysis of implant degradation. (A) Micro-computed tomography three-dimensional reconstruction of the Zn–Mg–Fe alloy implanted in the frontal bone, mandible, and femur, 3, 6, 9, and 12 months post surgery. (B) Volume loss of the Zn–Mg–Fe alloy implanted in the frontal bone, mandible, and femur, 3, 6, 9, and 12 months post surgery. (C) Corrosion rates of the Zn–Mg–Fe alloy implanted in the frontal bone, mandible, and femur, 3, 6, 9, and 12 months post surgery. For each data point, six samples were analyzed in duplicate, and the mean values $\pm$ SDs are presented. Scale bar = 10 mm. No statistically significant differences were observed in the volume loss or corrosion rates among the Zn–Mg–Fe alloy implanted in the frontal bone, mandible, and femur at the same time points analyzed ($p > 0.05$).

disrupt cytokine-mediated cell communication and impair the innate host defenses [45]. Accordingly, we here assessed the effects of the Zn–Mg–Fe alloy degradation using sensitive blood indicators, such as the CD4/CD8a lymphocyte ratio, and blood IL-2 and IL-4 levels. We found no adverse effects of the implanted alloy on the immune system.

Many factors affect the complex biodegradation environment *in vivo*, such as cells, pH, temperature, electrolyte flow, blood, and proteins [46–48]. Hence, the degradation of the Zn–Mg–Fe alloy should be tested *in vivo* to allow substantiated conclusions. Indeed, many studies have confirmed that the implantation site is an important factor influencing the degradation. For instance, Zhang et al. [49] found that a Mg alloy

implant degrades faster in the marrow channel than in the cortical bone. As another example, Willbold et al. [50] reported that the head of an AZ31 screw covered by soft tissue degrades faster than the screw threads in the hip bone in sheep. Therefore, determining the degradation of medical degradable materials in different physiological environments *in vivo* is crucial for identifying the most suitable materials for use in such specific physiological environments.

Bowen et al. [51] were the first to implant a pure zinc stent in the rat artery. They found that its degradation rate is uniform and close to the ideal stent degradation rate of 0.02 mm y^{-1} in the first 2–3 months after implantation, and accelerates afterwards. In the recent years, the use of

Table 2
Corrosion rate (mm y^{-1})[a].

Time after surgery (months)				
	3	6	9	12
Frontal bone	0.183 ± 0.017	0.106 ± 0.025	0.080 ± 0.006	0.065 ± 0.004
Mandible implant	0.164 ± 0.030	0.102 ± 0.020	0.080 ± 0.029	0.063 ± 0.003
Femur implant	0.169 ± 0.020	0.094 ± 0.013	0.080 ± 0.009	0.064 ± 0.005
p-value	0.3418	0.5340	0.9990	0.7477

[a] The corrosion rate was determined as described in section 2.8. The values are presented as the means ± SDs (n = 6).

zinc alloys as bone implants has gained increasing attention. Guo et al. [52] reported that pure zinc membranes implanted in rat cranium have a degradation rate of 0.044 ± 0.003 mm year^{-1}. Yang et al. [53] reported the degradation rate of 0.14 ± 0.05 mm year^{-1} for pure Zn in the rat femur after an 8-week implantation, with a relatively faster degradation rate of Zn-0.4Fe and Zn-0.8 Mg alloys. In the current study, we investigated the degradation of the Zn–Mg–Fe alloy used as an osteosynthesis system. We found that the corrosion rate reached 0.183 mm y^{-1} in the first 3 months and 0.065 mm y^{-1} at 12 months. Although slight differences were observed in the degradation of the Zn–Mg–Fe alloy in the frontal bone, mandible, and femur, they were not statistically significant. The implantation sites of the Zn–Mg–Fe alloy were all on the cortical bone surface covered by the periosteum. Hence, the tissues in direct contact with the Zn–Mg–Fe alloy may play a decisive role in its degradation.

Some studies examined the degradation products of zinc alloys used

as vascular stents. Zhao et al. [54] implanted a Zn–Li alloy in the rat abdominal aorta. Elemental mapping and FTIR analysis revealed calcium phosphate, zinc oxide, zinc chloride hydroxide, and zinc carbonate as the corrosion products. Drelich et al. [55] reported that zinc wires implanted in the murine artery show a steady degradation without local toxicity 20 months post implantation, and that zinc oxide, zinc carbonate, and zinc phosphate are the main components of the corrosion products. Degradation products have been also considered in studies into bone implants. For example, Yang et al. [56] reported that Zn, O, and P are the main components of the corrosion products of Zn and Zn–5Mg in rat femoral condyles. Further, Su et al. [57] demonstrated formation of a segmental layer of ZnP mosaicked with Zn(OH)$_2$ and ZnO at the implant/bone interface in a rat femur condyle model. In addition, He et al. [58] used in situ site-specific focused ion beam (FIB) micromilling and transmission electron microscopy (TEM) to analyze degradation products in the femur mid-diaphysis in New Zealand white rabbit. They reported the presence of porous Fe@Zn bone scaffolds with dominantly equiaxed nanocrystalline ZnO with a small amount of dispersed ZnCO$_3$. Finally, Guo et al. [52] reported that the thin inner layer of the degradation products adjacent to the surface of zinc matrix is rich in Zn and O, while the outer layer is mainly composed of P and Ca. In the current study, XPS, FITR, and XRD analyses revealed that the degradation products contain ZnO, Zn(OH)$_2$, Zn$_5$(OH)$_6$(CO$_3$)$_2$, and Zn$_3$(PO$_4$)$_2$·4H$_2$O, which was consistent with previous studies.

Pure zinc is reactive. In the initial stage of its degradation, it reacts with water forming Zn(OH)$_2$ and ZnO, without gas formation (equations (1)–(4)). The stability of Zn(OH)$_2$ and ZnO is determined by environmental factors, such as the type and concentration of ions and the concentration of degradation products [59]. The degradation product Zn(OH)$_2$ has anti-corrosive properties, which gradually slow down the
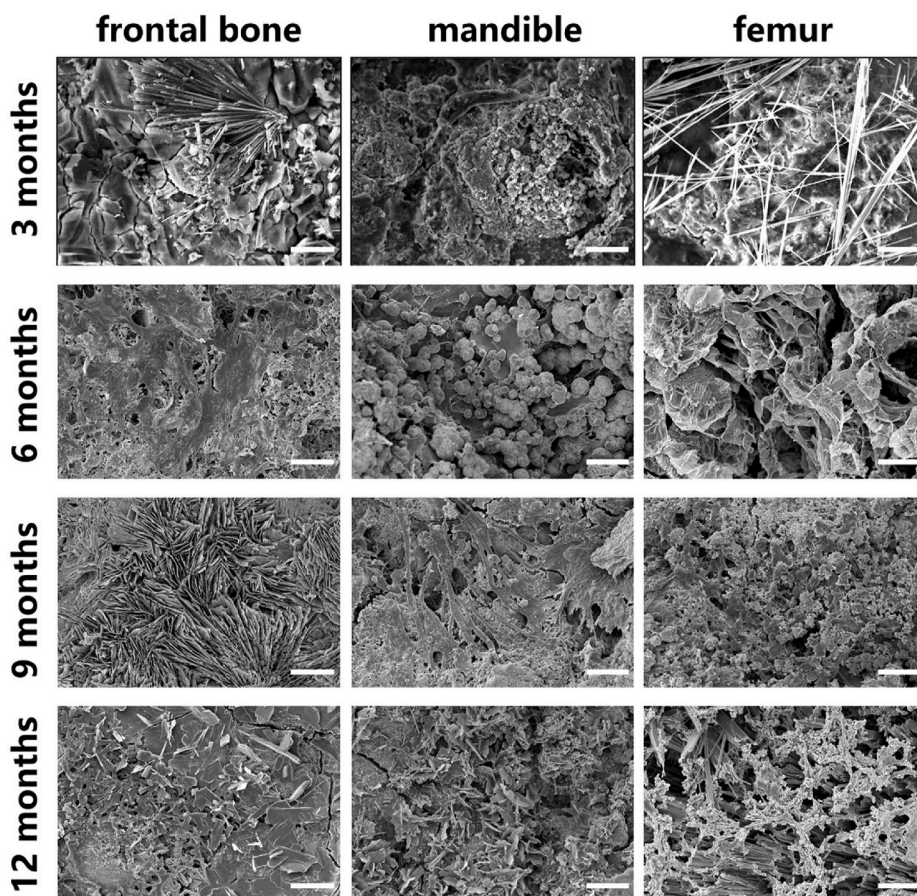

Fig. 7. Surface morphology of the Zn–Mg–Fe alloy implanted in the frontal bone, mandible, and femur, 3, 6, 9, and 12 months after implantation. Scale bar = 20 μm.
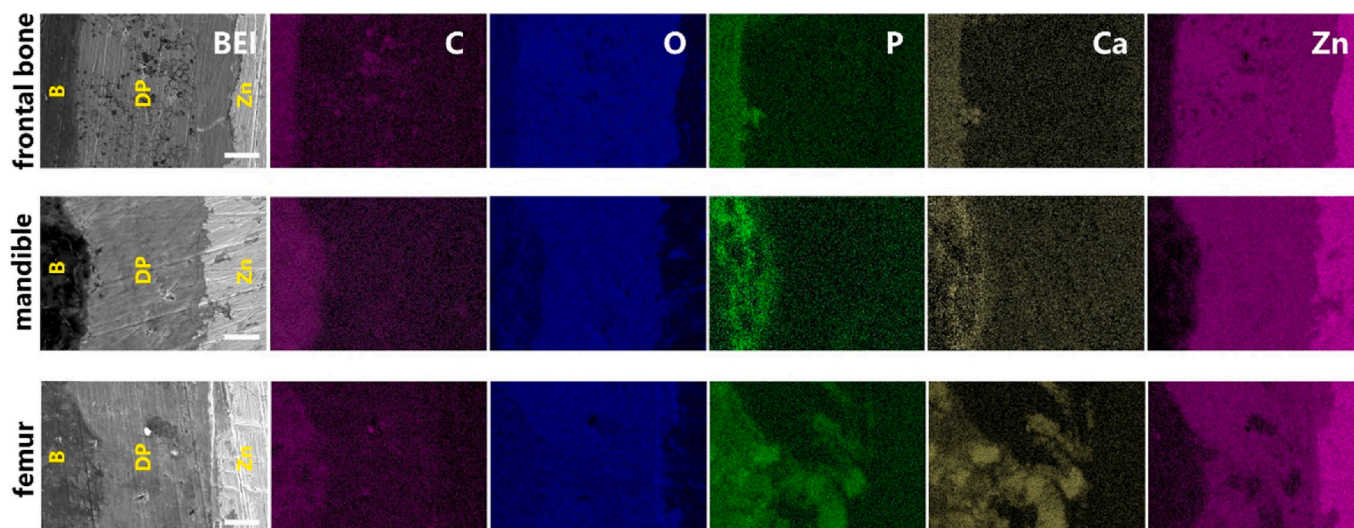
Fig. 8. Scanning electron microscopy images of the frontal bone, mandible, and femur cross-sections 12 months post surgery, and corresponding elemental distribution mapping. Carbon: C, purple; oxygen: O, blue; phosphate: P, green; calcium: Ca, yellow; zinc: Zn, pink; B: bone; DP: degradation products. Scale bar = 20 μm.
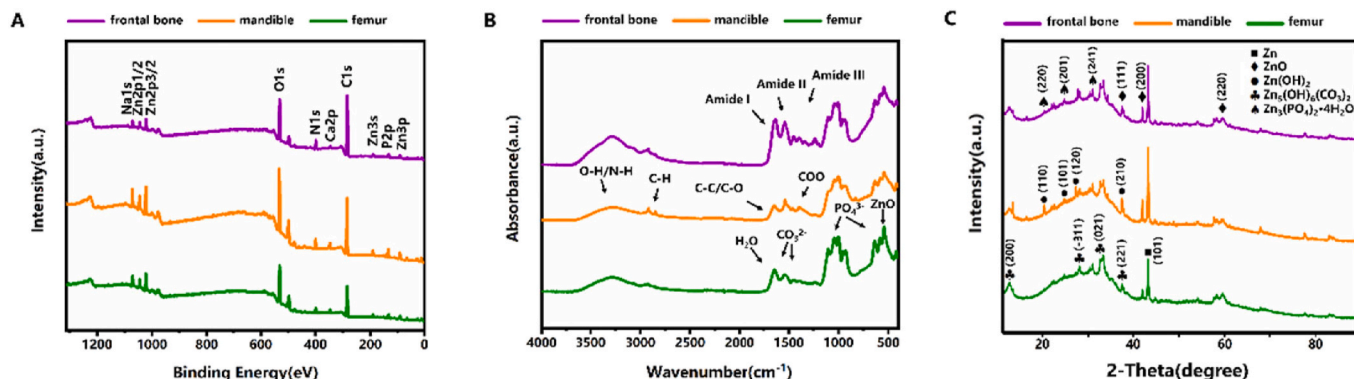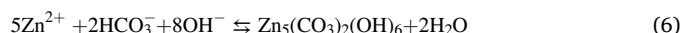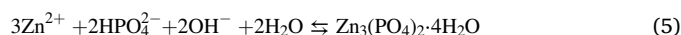

Fig. 9. Degradation product analysis. (A) X-ray photoelectron spectroscopy spectra, (B) Fourier-transform infrared spectra, and (C) X-ray diffraction patterns of the alloy degradation products 12 months post surgery.

degradation of the Zn–Mg–Fe alloy. Chloride ions can dissolve the insoluble $Zn(OH)_2$, and form insoluble phosphate and carbonate compounds [60,61](equations (5) and (6)). The inert materials formed during zinc degradation may contain many components with different densities. They have low solubility in body fluids and are physically deposited on the metal surface, hindering the degradation of the zinc alloy and slowing down the degradation rate [62]. In the current study, the degradation rate of the Zn–Mg–Fe alloy in the first 3 months after implantation was significantly faster than that in the latter 9 months probably because insoluble degradation products did not accumulate on the Zn–Mg–Fe alloy surface at the initial stage, allowing full contact between the Zn–Mg–Fe alloy materials and the microenvironment. Three months later, with the accumulation of insoluble degradation products, the degradation of the Zn–Mg–Fe alloy was hindered, resulting in a slow and uniform degradation of the implant. Since the observation time in the current study was 12 months, the *in vivo* degradation properties of the Zn–Mg–Fe alloy should in the future be evaluated in the longer term.

$$Zn \rightarrow Zn^{2+} + 2e^- \tag{1}$$

$$O_2 + 2H_2O + 4e^- \rightarrow 4OH^- \tag{2}$$

$$Zn^{2+} + 2OH^- \leftrightarrows Zn(OH)_2 \tag{3}$$

$$Zn(OH)_2 \leftrightarrows ZnO + H_2O \tag{4}$$

$$3Zn^{2+} + 2HPO_4^{2-} + 2OH^- + 2H_2O \leftrightarrows Zn_3(PO_4)_2 \cdot 4H_2O \tag{5}$$

$$5Zn^{2+} + 2HCO_3^- + 8OH^- \leftrightarrows Zn_5(CO_3)_2(OH)_6 + 2H_2O \tag{6}$$

After zinc alloy implantation *in vivo*, foreign body reaction and trauma are initiated, to form hematoma and elicit inflammatory response [63,64]. Cells (macrophages, foreign body giant cells, neutrophils, osteoblasts, stem cells, etc.), body fluid, proteins, and inorganic ions are deposited on the implant [65]. Degradation rate is relative rapid at this stage, with large amounts of Zn ions released [58]. Consequently, the inhibitory effect of Zn ions is predominant [66], and zinc content in the adjacent bone tissue rises significantly (Fig. 4).

Insoluble degradation products deposited on the surface of the Zn–Mg–Fe alloy resulted in a decreased concentration of zinc ions. Moderate zinc levels are beneficial for bone formation [67]. Zhu et al. [6] reported that zinc ions promote hMSC osteogenesis through TRPM7 and GPR39 receptors, activation of intracellular cAMP and PKA, and AKT and MARK activation. Yamaguchi et al. [68] reported that Zn stimulates osteoblastogenesis and suppresses osteoclastogenesis by antagonizing NF-κB activation. The connective tissue forms on the implant surface and is gradually replaced by new bone on the outer side of the connective tissue [57]. Mg and Fe ions are thought to play a minor role in the osseointegration of Zn–Mg–Fe alloy as compared to Zn ions, since the Mg and Fe levels were low, and EDS and XPS analyses detected

only trace amounts of these elements (Fig. 9, Fig. S3).

Following osseointegration, the tissue microenvironment changes to allow oxygen reduction, restrict fluid flow, impede mass exchange, and increase local pH, which, together with the formed insoluble degradation products, retard degradation rate. A decreased degradation rate with prolonged implantation time was also reported for the Zn–5Mg alloy [56]. A reduced release of Zn ions favors stimulation of new bone formation [66]. As shown in Fig. 8 in the current study, a region rich in Ca and P formed in the degradation product layer, which was considered to be a new bone, and indicated that new bone gradually replaces the degradation products. Tight and direct bone bonding of the Zn–Mg–Fe alloy allowed good bonding strength, avoiding implant loosening [58].

A uniform degradation of the Zn–Mg–Fe alloy was observed in the current study. Many visible and invisible pits and cracks can form during degradation of degradable alloys. The formation of these structures may greatly impact the performance of the degradable alloy as an osteosynthesis system material, leading to the decline of the mechanical implant integrity. Stress concentration may occur at the pits and cracks before early bone tissue healing and repair, hindering bone remodeling and biological function recovery, resulting in fixation failure. Hence, developing degradable alloys that are suitable for the local microenvironment is important [69].

In the current study, we followed the *in vivo* degradation of the Zn–Mg–Fe alloy in the first 12 months of implantation. In the future, we plan to track its complete degradation. If the insoluble substances on the implant surface retard the implant degradation, future studies should focus on how to improve or maintain a uniform degradation rate in the later stages of implantation. Furthermore, the mechanism by which the Zn–Mg–Fe alloy is metabolized in the body should be studied further. In addition, we here investigated the degradation differences of the Zn–Mg–Fe alloy as an osteosynthesis system on the bone surface in the frontal bone, mandible, and femur, but did not consider other orthopedic devices, such as intramedullary nails. Finally, the potential applications of degradable metals *in vivo*, such as the subcutaneous, muscle, urethra, intestine, and heart applications, should also be investigated.

5. Conclusions

In the current study, we performed a detailed evaluation of the biocompatibility and degradation of a Zn–Mg–Fe alloy used as an osteosynthesis system in the frontal bone, mandible, and femur in beagle, for 1 year. The analysis indicated good compatibility of the Zn–Mg–Fe alloy, with limited toxicity *in vivo*. Bone zinc content significantly increased in 3 months post implantation, and then decreased, which was related to the degradation of the Zn–Mg–Fe alloy. The Zn–Mg–Fe alloy was degraded in a uniform manner, with no significant differences in the degradation rate among the frontal bone, mandible, and femur implants. The degradation rate reached approximately 0.183 mm y^{-1} in the first 3 months, and then decreased to approximately 0.065 mm y^{-1} at 12 months. The degradation products were zinc oxide [ZnO], zinc hydroxide [Zn(OH)$_2$], hydrozincite [Zn$_5$(OH)$_6$(CO$_3$)$_2$], and hopeite [Zn$_3$(PO$_4$)$_2$·4H$_2$O]. A trend of degradation product replacement by the bone was observed, allowing implant stabilization in the long term. In conclusion, the study revealed that with good biocompatibility, mechanical strength, and degradation properties, the Zn–Mg–Fe alloy is a promising candidate for an osteosynthesis system.

CRediT authorship contribution statement

Xiaoxi Shao: Conceptualization, Methodology, Investigation, Validation, Formal analysis, Writing – original draft, Writing – review & editing. **Xiang Wang:** Methodology, Investigation, Validation, Formal analysis, Writing – review & editing. **Fangfang Xu:** Methodology, Investigation, Validation, Formal analysis, Writing – review & editing. **Taiqiang Dai:** Methodology, Investigation, Validation, Formal analysis,

Writing – review & editing. **Jack G. Zhou:** Methodology, Validation, Formal analysis, Writing – review & editing. **Jiang Liu:** Methodology, Investigation, Validation, Formal analysis, Funding acquisition. **Kun Song:** Methodology, Investigation, Validation, Formal analysis. **Lei Tian:** Conceptualization, Methodology, Formal analysis, Resources, Writing – original draft, Project administration, Funding acquisition, Supervision, Writing – review & editing. **Bin Liu:** Conceptualization, Methodology, Formal analysis, Resources, Writing – original draft, Project administration, Funding acquisition, Supervision, Writing – review & editing. **Yanpu Liu:** Conceptualization, Methodology, Formal analysis, Resources, Writing – original draft, Project administration, Funding acquisition, Supervision, Writing – review & editing.

Declaration of competing interest

None.

Acknowledgments

Appendix A. Supplementary data

Supplementary data to this article can be found online at https://doi.org/10.1016/j.bioactmat.2021.05.012.

References

[1] J. Venezuela, M.S. Dargusch, The influence of alloying and fabrication techniques on the mechanical properties, biodegradability and biocompatibility of zinc: a comprehensive review, Acta Biomater. 87 (2019) 1–40.

[2] E. Mostaed, M. Sikora-Jasinska, J.W. Drelich, M. Vedani, Zinc-based alloys for degradable vascular stent applications, Acta Biomater. 71 (2018) 1–23.

[3] H. Yang, B. Jia, Z. Zhang, X. Qu, G. Li, W. Lin, D. Zhu, K. Dai, Y. Zheng, Alloying design of biodegradable zinc as promising bone implants for load-bearing applications, Nat. Commun. 11 (1) (2020) 401.

[4] J. Lin, X. Tong, Z. Shi, D. Zhang, C. Wen, A biodegradable Zn-1Cu-0.1Ti alloy with antibacterial properties for orthopedic applications, Acta Biomater. 106 (2020) 410–427.

[5] Y. Su, I. Cockerill, Y. Wang, Y.X. Qin, L. Chang, Y. Zheng, D. Zhu, Zinc-based biomaterials for regeneration and therapy, Trends Biotechnol. 37 (4) (2019) 428–441.

[6] D. Zhu, Y. Su, M.L. Young, J. Ma, Y. Zheng, L. Tang, Biological responses and mechanisms of human bone marrow mesenchymal stem cells to Zn and Mg biomaterials, ACS Appl. Mater. Interfaces 9 (33) (2017) 27453–27461.

[7] H.R. Bakhsheshi-Rad, E. Hamzah, H.T. Low, M. Kasiri-Asgarani, S. Farahany, E. Akbari, M.H. Cho, Fabrication of biodegradable Zn-Al-Mg alloy: mechanical properties, corrosion behavior, cytotoxicity and antibacterial activities, Mater Sci Eng C Mater Biol Appl 73 (2017) 215–219.

[8] Y.F. Zheng, X.N. Gu, F. Witte, Biodegradable metals, Mater. Sci. Eng. R Rep. 77 (2014) 1–34.

[9] D. Vojtech, J. Kubasek, J. Serak, P. Novak, Mechanical and corrosion properties of newly developed biodegradable Zn-based alloys for bone fixation, Acta Biomater. 7 (9) (2011) 3515–3522.

[10] X. Wang, X. Shao, T. Dai, F. Xu, J.Y. Liu, In vivo study of the efficacy, biosafety, and degradation of a zinc alloy osteosynthesis system, Acta Biomater. 94 (2019) 351–361.

[11] L.R. Laura M Plum, Hajo Haase, The essential toxin: impact of zinc on human health, Int. J. Env. Res. Public Health Apr 7 (4) (2010) 1342–1365.

[12] J. Osredkar, Copper and zinc, biological role and significance of copper/zinc imbalance, J. Clin. Toxicol. s3 (1) (2011).

[13] P. Whittaker, Iron and zinc interactions in humans, Am. J. Clin. Nutr. 68 (suppl) (1998) 442S, 6S.

[14] P.L. Hooper, L. Visconti, P.J. Garry, G.E. Johnson, Zinc lowers high-density lipoprotein-cholesterol levels, J. Am. Med. Assoc. 244 (17) (1980) 1960–1961.

[15] N. Wijesekara, F. Chimienti, M.B. Wheeler, Zinc, a regulator of islet function and glucose homeostasis, Diabetes Obes. Metabol. 11 (4) (2010) 202–214.

[16] M.K. Mohammad, Z. Zhou, M. Cave, A. Barve, C.J. McClain, Zinc and liver disease, Nutr. Clin. Pract. 27 (1) (2012) 8–20.

[17] Atish Prakash, Kanchan Bharti, Abu Bakar, A. Majeed, Zinc: indications in brain disorders, Fundam. Clin. Pharmacol. 29 (2) (2015) 131–149.

[18] P.A.A. Stuart D Portbury, Zinc signal in brain disease, Int. J. Mol. Sci. 18 (12) (2017) 2506.

[19] J. Zhao, Q. Wu, X. Hu, X. Dong, L. Wang, Q. Liu, Z. Long, L. Li, Comparative study of serum zinc concentrations in benign and malignant prostate disease: a Systematic Review and Meta-Analysis, For. Rep. 6 (1) (2016) 25778.

[20] R.K. Chandra, Excessive intake of zinc impairs immune responses, J. Am. Med. Assoc. 252 (11) (1984) 1443–1446.

[21] C. Miura, Y. Shimizu, Y. Imai, T. Mukai, A. Yamamoto, Y. Sano, N. Ikeo, S. Isozaki, T. Takahashi, M. Oikawa, H. Kumamoto, M. Tachi, In vivo corrosion behaviour of magnesium alloy in association with surrounding tissue response in rats, Biomed. Mater. 11 (2) (2016), 025001.

[22] E. Willbold, A.A. Kaya, R.A. Kaya, F. Beckmann, F. Witte, Corrosion of magnesium alloy AZ31 screws is dependent on the implantation site, Mater. Sci. Eng., B 176 (20) (2011) 1835–1840.

[23] F. Witte, N. Hort, C. Vogt, S. Cohen, K.U. Kainer, R. Willumeit, F. Feyerabend, Degradable biomaterials based on magnesium corrosion, Curr. Opin. Solid State Mater. Sci. 12 (5–6) (2008) 63–72.

[24] E.d. Lahunta, Miller's Anatomy of the Dogs, 2012.

[25] X. Wang, X. Shao, T. Dai, F. Xu, J.G. Zhou, G. Qu, L. Tian, B. Liu, Y. Liu, In vivo study of the efficacy, biosafety, and degradation of a zinc alloy osteosynthesis system, Acta Biomater. 92 (2019) 351–361.

[26] M.P. Staiger, A.M. Pietak, J. Huadmai, G. Dias, Magnesium and its alloys as orthopedic biomaterials: a review, Biomaterials 27 (9) (2006) 1728–1734.

[27] R. Brian, Strohmeier, M. David, Hercules, Surface spectroscopic characterization of the interaction between zinc ions and γ-alumina, J. Catal. 86 (2) (1984) 266–279.

[28] Characterization of calcium-modified zinc phosphate conversion coatings and their influences on corrosion resistance of AZ31 alloy, Surf. Coating. Technol. 205 (11) (2011) 3347–3355.

[29] W.F. Stratmann, The delamination of polymeric coatings from electrogalvanised steel – a mechanistic approach.: Part 1: delamination from a defect with intact zinc layer, Corrosion Sci. 43 (2) (2001) 227.

[30] K. Torne, A. Ornberg, J. Weissenrieder, Influence of strain on the corrosion of magnesium alloys and zinc in physiological environments, Acta Biomater. 48 (2017) 541–550.

[31] M. Ascencio, M. Pekguleryuz, S. Omanovic, An investigation of the corrosion mechanisms of WE43 Mg alloy in a modified simulated body fluid solution: the influence of immersion time, Corrosion Sci. 87 (2014) 489–503.

[32] H. Guo, D. Xia, Y. Zheng, Y. Zhu, Y. Liu, Y. Zhou, A pure zinc membrane with degradability and osteogenesis promotion for guided bone regeneration: in vitro and in vivo studies, Acta Biomater. 106 (2020) 396–409.

[33] A. Barth, Infrared spectroscopy of proteins, Biochim. Biophys. Acta 1767 (9) (2007) 1073–1101.

[34] X. Liu, H. Yang, Y. Liu, P. Xiong, H. Guo, H.H. Huang, Y. Zheng, Comparative studies on degradation behavior of pure zinc in various simulated body fluids, JOM (J. Occup. Med.) 71 (2019) 1414–1425.

[35] H. Tapiero, K.D. Tew, Trace elements in human physiology and pathology: zinc and metallothioneins, Biomed. Pharmacother. 57 (9) (2003) 399–411.

[36] C.W.L. Deborah R Morris, Neurotoxicity of zinc, Adv Neurobiol 18 (2017) 303–312.

[37] L.M. Plum, L. Rink, H. Haase, The essential toxin: impact of zinc on human health, Int. J. Environ. Res. Publ. Health 7 (4) (2010) 1342–1365.

[38] E.S. Eshak, K. Iso, K. Yamagishi, K. Maruyama, M. Umesawa, A. Tamakoshi, Associations between copper and zinc intakes from diet and mortality from cardiovascular disease in a large population-based prospective cohort study, J. Nutr. Biochem. (2018) 126.

[39] C. Rossig, N. Angrisani, P. Helmecke, S. Besdo, J.M. Seitz, B. Welke, N. Fedchenko, H. Kock, J. Reifenrath, In vivo evaluation of a magnesium-based degradable intramedullary nailing system in a sheep model, Acta Biomater. 25 (2015) 369–383.

[40] L. Xu, G. Yu, E. Zhang, F. Pan, K. Yang, In vivo corrosion behavior of Mg-Mn-Zn alloy for bone implant application, J. Biomed. Mater. Res. 83 (3) (2007) 703–711.

[41] F. Amerstorfer, S.F. Fischerauer, L. Fischer, J. Eichler, J. Draxler, A. Zitek, M. Meischel, E. Martinelli, T. Kraus, S. Hann, S.E. Stanzl-Tschegg, P.J. Uggowitzer, J.F. Loffler, A.M. Weinberg, T. Prohaska, Long-term in vivo degradation behavior and near-implant distribution of resorbed elements for magnesium alloys WZ21 and ZX50, Acta Biomater. 42 (2016) 440–450.

[42] M. Maares, H. Haase, Zinc and immunity: an essential interrelation, Arch. Biochem. Biophys. 611 (2016) 58–65.

[43] T.F. Shintaro, Hojyo roles of zinc signaling in the immune system, J Immunol Res 2016 (2016) 6762343.

[44] I. Wessels, M. Maywald, L. Rink, Zinc as a gatekeeper of immune function, Nutrients 9 (12) (2017) 1286.

[45] K. Grungreiff, D. Reinhold, Zinc: a complementary factor in the treatment of chronic hepatitis C? (Review), Mol. Med. Rep. 3 (3) (2010) 371–375.

[46] M. Mouanga, P. Berçot, J.Y. Rauch, Comparison of corrosion behaviour of zinc in NaCl and in NaOH solutions. Part I: corrosion layer characterization, Corrosion Sci. 52 (12) (2010) 3984–3992.

[47] M. Mouanga, P. Berot, Comparison of corrosion behaviour of zinc in NaCl and in NaOH solutions; Part II: electrochemical analyses, Corrosion Sci. 52 (12) (2010) 3993–4000.

[48] L. Liu, Y. Meng, A.A. Volinsky, H.J. Zhang, L.N. Wang, Influences of albumin on in vitro corrosion of pure Zn in artificial plasma, Corrosion Sci. 153 (JUN) (2019) 341–356.

[49] E. Zhang, L. Xu, G. Yu, F. Pan, K. Yang, In vivo evaluation of biodegradable magnesium alloy bone implant in the first 6 months implantation, J. Biomed. Mater. Res. 90 (3) (2009) 882–893.

[50] K.A.A. Willbold E, R.A. Kaya, F. Beckmann, F. Witte, Corrosion of magnesium alloy AZ31 screws is dependent on the implantation site, Mater. Sci. Eng. B 176 (2011) 1835–1840.

[51] P.K. Bowen, J. Drelich, J. Goldman, Zinc exhibits ideal physiological corrosion behavior for bioabsorbable stents, Adv. Mater. 25 (18) (2013) 2577–2582.

[52] H. Guo, D. Xia, Y. Zheng, Y. Zhu, Y. Zhou, A pure zinc membrane with degradability and osteogenesis promotion for guided bone regeneration: in vitro and in vivo studies, Acta Biomater. 106 (9) (2020).

[53] H. Yang, B. Jia, Z. Zhang, X. Qu, Y. Zheng, Alloying design of biodegradable zinc as promising bone implants for load-bearing applications, Nat. Commun. 11 (1) (2020) 401.

[54] S. Zhao, J.M. Seitz, R. Eifler, H.J. Maier, R.J. Guillory 2nd, E.J. Earley, A. Drelich, J. Goldman, J.W. Drelich, Zn-Li alloy after extrusion and drawing: structural, mechanical characterization, and biodegradation in abdominal aorta of rat, Mater Sci Eng C Mater Biol Appl 76 (2017) 301–312.

[55] A.J. Drelich, S. Zhao, R.J. Guillory 2nd, J.W. Drelich, J. Goldman, Long-term surveillance of zinc implant in murine artery: surprisingly steady biocorrosion rate, Acta Biomater. 58 (2017) 539–549.

[56] H. Yang, X. Qu, W. Lin, D. Chen, D. Zhu, K. Dai, Y. Zheng, Enhanced osseointegration of Zn-Mg composites by tuning the release of Zn ions with sacrificial Mg-rich anode design, ACS Biomater. Sci. Eng. 5 (2) (2018) 453–467.

[57] Y. Su, H. Yang, J. Gao, Y. Qin, Y. Zheng, D. Zhu, Interfacial zinc phosphate is the Key to controlling biocompatibility of metallic zinc implants, Advanced Science 6 (14) (2019) 1900112.

[58] J. He, J. Fang, P. Wei, Y. Li, F. Ren, Cancellous bone-like porous Fe@Zn scaffolds with core-shell-structured skeletons for biodegradable bone implants, Acta Biomater. 121 (7) (2020) 665–681.

[59] I.C. Th Muster, The protective nature of passivation films on zinc: surface charge, Corrosion Sci. 47 (7) (2005) 1861–1862.

[60] X.G. Zhang, Corrosion and Electrochemistry of Zinc, Springer Science & Business Media, 2013.

[61] Z.W. Chen Y, M.F. Maitz, et al., Comparative corrosion behavior of Zn with Fe and Mg in the course of immersion degradation in phosphate buffered saline, Corrosion Sci. 111 (2016) 541–555.

[62] Y. Jang, B. Collins, J. Sankar, Y. Yun, Effect of biologically relevant ions on the corrosion products formed on alloy AZ31B: an improved understanding of magnesium corrosion, Acta Biomater. 9 (10) (2013) 8761–8770.

[63] J.M. Anderson, A. Rodriguez, D.T. Chang, Foreign body reaction to biomaterials, Semin. Immunol. 20 (2) (2008) 86–100.

[64] R. Klopfleisch, F. Jung, The pathology of the foreign body reaction against biomaterials, J. Biomed. Mater. Res. 105 (3) (2017) 927.

[65] R. Trindade, T. Albrektsson, P. Tengvall, A. Wennerberg, Foreign Body Reaction to Biomaterials: on Mechanisms for Buildup and Breakdown of Osseointegration, Clinical Implant Dentistry & Related Research, 2016, pp. 192–203.

[66] H. Yang, X. Qu, W. Lin, C. Wang, D. Zhu, K. Dai, Y. Zheng, In vitro and in vivo studies on zinc-hydroxyapatite composites as novel biodegradable metal matrix composite for orthopedic applications, Acta Biomater. 71 (2018) 200–214.

[67] Y. Song, H. Wu, Y. Gao, J. Li, G. Pei, Zinc silicate/nano-hydroxyapatite/collagen scaffolds promote angiogenesis and bone regeneration via the p38 MAPK pathway in activated monocytes, ACS Appl. Mater. Interfaces 12 (14) (2020) 16058–16075.

[68] M. Yamaguchi, M.N. Weitzmann, Zinc stimulates osteoblastogenesis and suppresses osteoclastogenesis by antagonizing NF-κB activation, Mol. Cell. Biochem. 355 (1–2) (2011) 179.

[69] D. Zhao, F. Witte, F. Lu, J. Wang, J. Li, L. Qin, Current status on clinical applications of magnesium-based orthopaedic implants: a review from clinical translational perspective, Biomaterials 112 (2017) 287–302.